Supporting Material

1 Cell contraction speed

Our model of cell motility is based on the assumption of a constant contraction rate. In particular, we assume that the contraction is not hindered by the opposing forces exerted by the stretched binding bridges and that, based on experimental data, the relevant contraction rates are around $\sim 10\mu m\,\mathrm{min}^{-1}$, which are much smaller than the speed of single myosin heads ($\sim 1\mu m\,\mathrm{sec}^{-1}$ [1]). In this section we discuss this assumption and show that the main results can be reproduced with a force-dependent contraction rate with suitably chosen parameters.

The total force F_μ exerted by the myosin motors has to balance both the resistive force due to the binding bridges F_b and the viscous drag F_ν of the cytoplasmic flow caused by the deformation:

$$F_\mu = F_b + F_\nu \ . \tag{1}$$

Based on *in vitro* data of the velocity-load relationship of muscle myosin [2], we assume that the total force of all myosins engaged in cell contraction can be approximated by a linear velocity-load dependence

$$F_\mu = F_s - \frac{F_s}{v_0} v \equiv F_s - \lambda v \ . \tag{2}$$

where F_s is the maximum, or stall, force, corresponding to the maximum force that can be generated by myosin. The viscous term in Eq. 1 can be written as

$$F_\nu = \nu\, v \ . \tag{3}$$

The force balance therefore leads to an expression for the speed

$$v = \frac{F_s - F_b}{\lambda + \nu} \ . \tag{4}$$

The parameters in this equation can be estimated from previous studies. The maximal force F_s can be estimated from the study of the speed of furrow ingression in cytokinesis [3]. There, the driving force was argued to be $F \sim 1\mathrm{nN}$, which can be viewed as a lower bound for the maximal force. The force exerted on the bindings is equal to the experimentally measured pole forces, i.e. $F_b \sim 0.2\mathrm{nN}$, and is five to ten times smaller than the maximal force. A single myosin moves freely with $v_0^{\mathrm{single}} \sim 1\mu m/s$ and stalls at $F_s^{\mathrm{single}} \sim 1\mathrm{pN}$, yielding $\lambda^{\mathrm{single}} \sim 10^{-6}\mathrm{N\,s\,m}^{-1}$. In the extreme case where all myosins pull on one filament in one direction we have $v_0 = v_0^{\mathrm{single}}$. For a stall force of $F_s \sim 1\mathrm{nN}$, see above, we find $\lambda \sim 10^{-3}\mathrm{N\,s\,m}^{-1}$. Note, however, that the number of motors in a cell is large, indicating that the organization of myosins is more complex. Thus, the total contraction velocity v_0 may be considerably lower than v_0^{single}.

To estimate the viscous drag, we follow Ref. [3] and model the cell as a cylinder of length $h_0 \sim 20\mu$m and radius $r \sim 5\mu$m that is compressed along its length axis. [1]. Using the results from Ref. [3] we find

$$v \equiv \dot{h} = -\frac{\sigma_{zz}}{3\mu} h(t) \ . \tag{5}$$

In our case, σ_{zz} is the contractile stress acting on the top and bottom of the cylinder, while $\mu \sim 300$Pa s is the cytoplasmic viscosity. The contractile force needed to balance the viscous stress is

$$F_\nu = \pi r^2 \sigma_{zz} = 3\pi \frac{r^2}{h} \mu v \equiv \nu v \tag{6}$$

with $\nu \sim 3 \cdot 10^{-3}$N s m^{-1}. In experiments, a contraction lasts for $\tau \sim 60$s and results in a length reduction $h_0 - h(\tau) \sim v\tau \sim 10\mu$m, giving $F_\nu \sim 0.5$nN.

The denominator in Eq. 4 represents a total friction term of order $\sim 10^{-3}$N s m^{-1}. In the case where the pole force can be neglected in comparison to the maximal force, force balance results in a constant contraction speed $v = F_s/(\nu + \mu) \sim 10^{-6}$m s^{-1} in agreement with experimental results [2]. However, pole forces can become comparable to the maximal force if the off-rate is very low. To investigate this effect we have performed simulations taking the relation Eq. 4 into account.

In a first set of simulations we have examined the effect of a stall force that is much larger than the maximal pole force. Specifically, we set $F_s = 10 k_s R$, which is approximately 10 times the maximal pole force observed for the standard parameter set, in agreement with above estimates. The load-free contraction velocity was chosen to be $v_0 \sim R/\tau \sim 10\mu$m min^{-1}, as in the old simulations. This choice of parameters corresponds to an effective friction of $(\nu + \lambda) \sim 6 \cdot 10^{-3}$N s m^{-1} in agreement with the above estimates.

The red solid line in Fig. S1(a) shows the cell speed as a function of the off-rate $k_{-,b}$ for these new simulations. The red dotted line is the curve from Fig 6d in the manuscript, i.e., for simulations in which the velocity was load-independent ($v = v_0$). The deviation between the two curves becomes significant only for very low off-rates. Moreover, both curves are rather flat and do not display the "biphasic" relationship seen in other studies [4]. The blue curve in Fig. S1(a) shows the maximum pole force for the new simulations. For low off-rates, this pole force approaches the stall force. In the load independent simulations presented in the main text, the radius r_f of the ellipse at the end of the contraction is fixed at $0.5R$. Now however, this radius is no longer fixed and depends on the off-rate. This is shown by the green curve which demonstrates that, as expected, r_f increases for decreasing values of the off-rate. Finally, we show in Fig. S2 the contraction speed v_{con} during the contraction cycle as a function of the off-rate using a color scale. The plot shows that

[1] This estimate neglects the *elastic* properties of the compressed material. Furthermore, it does not take into account that the cytoplasm has to flow through a porous medium. Also note that the force that opposes myosin-contraction may arise from the rupture of cross-links in the acto-myosin cortex itself and the reorganization of the cortex. To clarify this issue one should study the contraction of an isolated acto-myosin cortex patch (i.e. without cell attachments nor viscous drag). In this context one should also quantify the effect of myosin-crosslinking *vs* other cross-linking on cortical viscosity in myoII-null mutants.

[2] Note, that here the maximal force F_s results in cortical motion: The stalling of the myosins leads to a decrease of the viscous drag. The load on the motors in turn drops below F_s. Therefore, myosin motors can always operate at their total maximal force.

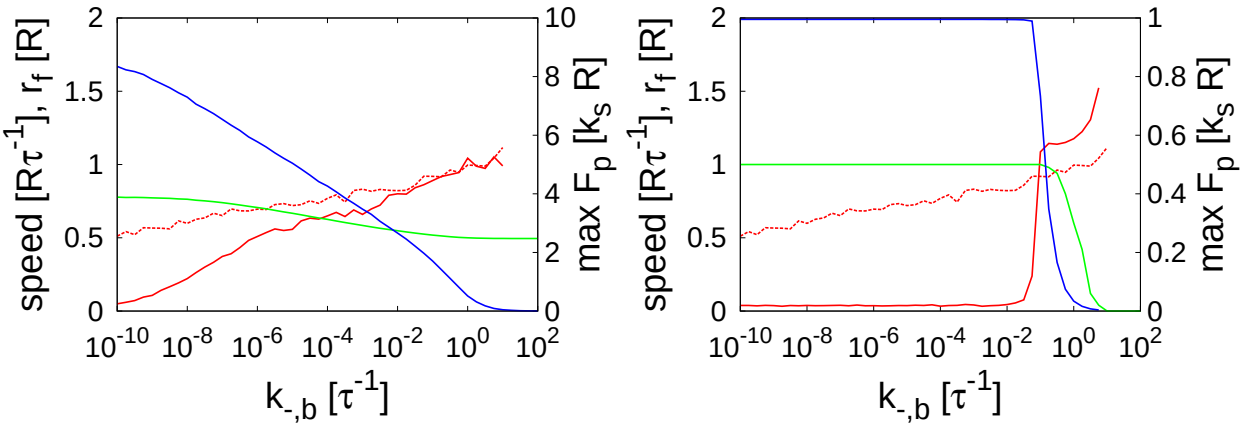

Figure 1: Cell speed as a function of the off-rate for (a) $F_s = 10 k_s R$, $v_0 = R\tau^{-1}$, (b) $F_s = 1 k_s R$, $v_0 = 10 R\tau^{-1}$. Red solid curve: cell speed when force-velocity relation is taken into account. Red dashed curve: cell speed with constant contraction speed. Green curve: Major axis of ellipse at end of contraction phase. Blue curve: maximal pole force during contraction.

v_{con} becomes only appreciably different from v_0 for very small off rates. For these values, the contraction velocity becomes small during the later stages of the contraction cycle. For most values of the off-rates, however, the contraction velocity is close to v_0 throughout the cycle.

In a second set of simulations, we examined the case of a stall force that was close to the maximal pole force in simulations with constant contraction speed and for the standard choice of parameters. Thus, we set $F_s = 1 k_s R$ corresponding to ≈ 1.1 times the maximal pole force. In order to obtain an effective contraction speed $v \sim 0.1 v_0$, we set $v_0 \sim 10 R/\tau \sim 1.6 \mu\mathrm{m\,sec}^{-1}$, corresponding to the speed of free myosin motors. Fig. S1(b) shows the cell speed as a function of the off-rate $k_{-,b}$ for these simulations. In contrast to the previous case, the pole force (blue curve) now reaches the stall force for small off-rates. This can be understood by realizing that the the stall force of $1\, k_s R$ is not large enough to cause a significant loss of attachments. In this regime, the contraction stalls completely shortly after onset, as indicated by the fact that the final radius approaches $r_f = 1$ (green curve) and that the contraction speed drops to 0. In contrast, for $k_{-,b}$ slightly larger than the standard choice ($k_{-,b} = 0.6\tau^{-1}$), the off-rate and the contraction rate is so large that the the ellipse contracts to a point. This can be clearly seen in the green curve which plots $r_f = 0$ as a function of the off-rate. Due to asymmetric detachment rates, the center of the ellipse is shifted to the right, leading to a cell speed larger than $1 R\tau^{-1}$.

In conclusion, we have shown that our main results still hold when a force-dependent contraction rate is taken into account, provided that the stall force is much larger than the pole force (see Fig. S1(a)). We estimate that the maximal contraction force that can be exerted by cellular myosin exceeds the typical pole forces observed in experiment. Moreover, we find that in this regime our model assumption of a constant

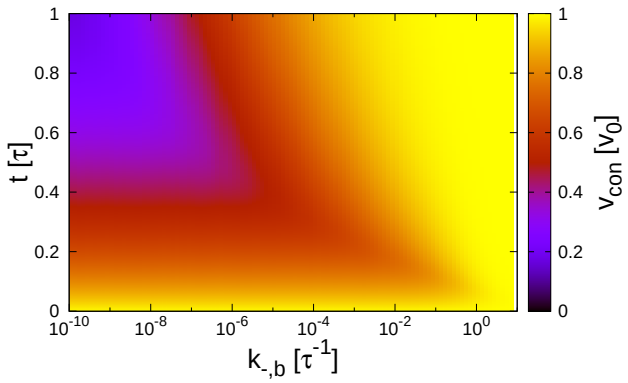

Figure 2: Contraction rate as a function of time and $k_{-,b}$ for $F_s = 10k_sR$, $v_0 = R\tau^{-1}$. The contraction rate is nearly constant over time for most off-rates.

contraction rate can be justified.

2 Further simulations results

In Fig. S3 we demonstrate how simulation data for a single cell relates to the average data discussed in the main text. The contact area at the beginning of the contraction phase is represented as an ellipse which is uniformly covered with attachment points (as in the ellipse at $t = 1.0$ in Fig. S3). The ellipse is contracted linearly in time and its position is adjusted according to the force balance of the binding bridges (resulting in the smaller ellipses in Fig. S3). From a single simulation run we collect the set of point forces as a function of time (black and green arrows) which are then averaged over an ensemble of 1000 runs to give average stress patterns (gray pattern). The position of the last focus (green arrow) is tracked in time (black line). Its position at the end of the cycle defines the rear most edge of the contact area at the start of the new cycle (ellipse at $t = 1.0$, compare also to Fig.1 (e) in the main text). The red curve shows the ensemble average of these curves. The average cell speed (which is plotted in Fig.6 in the main text) is defined as the average rear most position at the end of the cycle divided by the length of the cycle.

During the contraction phase, part of the cell-substratum bridges detach, see arrows in Fig. S3. Fig. S4 shows the ensemble average of distribution of attachment points (bridges) at different times. Parameter values are the same as used in Fig.3 in the main text. Clearly, only bridges close to the center of contraction remain at the end of the contraction phase. Note, that the center of contraction does not necessarily coincide with the center of the ellipse. Preferential detachment at the rear leads to a sideways shift of both the center of concentration and the contracted ellipse.

Fig. S5 shows the distribution of bridges averaged over time similar to the stress pattern in Fig.4 in the main text. Similar to the stress pattern, the bridge distribution depends most strongly on $k_{-,b}$, k_+, Δ and k_s. Clearly, the density decreases for increasing $k_{-,b}$ or decreasing k_+. The dimensionless parameter

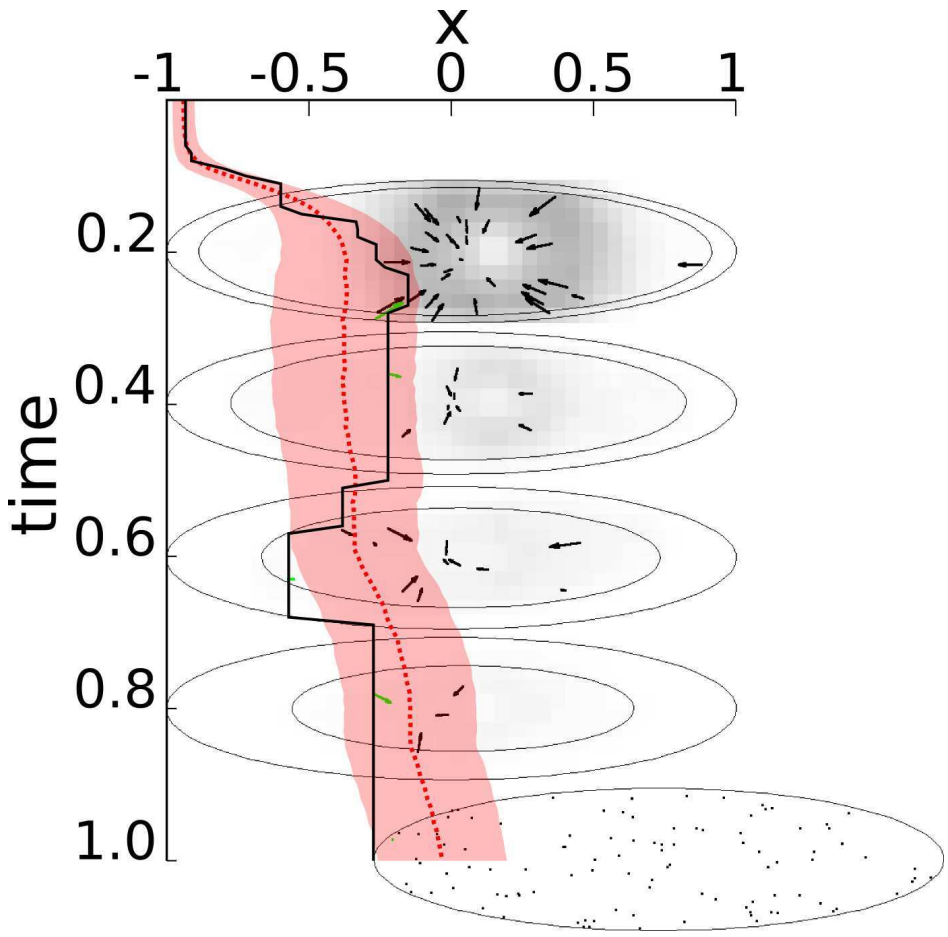

Figure 3: Overlay of single run data and ensemble average over 1000 independent runs for the standard parameter set. Shown are the average stress patterns for $t = 0.2, 0.4, 0.6, 0.8$, see also Fig. 3 in the main text. The size and shift of the contracted cell is indicated by the inner ellipses. Overlaid are force vectors for a single run, indicating also the discreteness of the attachment points. The force vector of the rear most focus at the respective time points for that single run is shown in green. The time course of this positions is shown as a black curve. The red curve and the red shaded area are the ensemble average of the position of the rear-most focus and its standard deviation, respectively. The new cycle starts with a new ellipse whose back coincides with the position of the last remaining focus from the previous cycle, as indicated by the ellipse at $t = 1.0$.

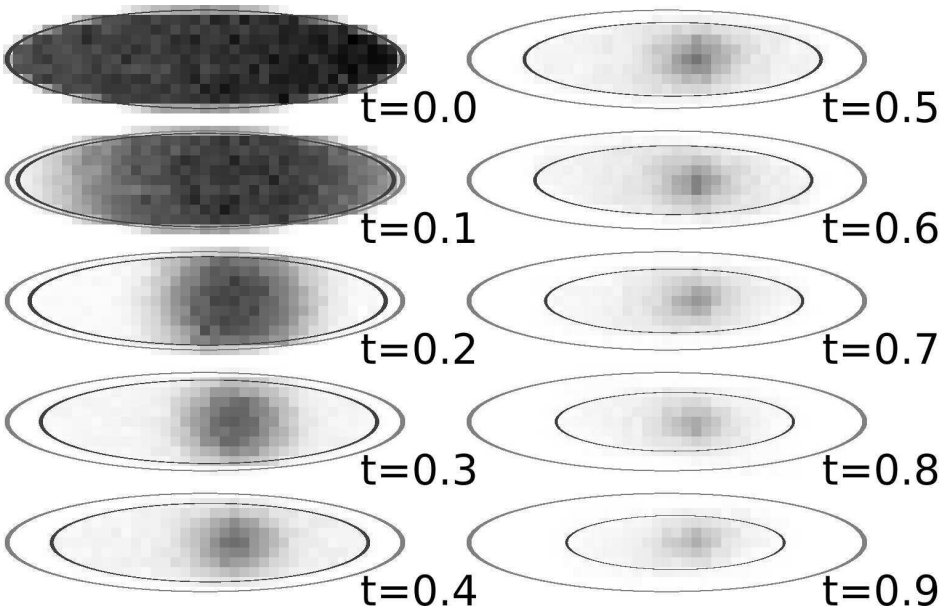

Figure 4: Average attachment distributions over 1000 simulation runs with time expressed in units of the contraction cycle. The attachment density is shown in a gray-scale with black corresponding to $\approx 1.8\mu\mathrm{m}^{-2}$.

$\alpha = Rk_s\Delta/(k_bT)$ controls the force dependent part of the detachment rate. A larger α speeds up detachment leading to a smaller average bridge density. Note, that unlike the stress pattern, the distribution of bridges does not scale with k_s. Rather it depends on k_s and Δ via α alone. In contrast to the stress pattern, the bridge density is strongly affected by the amount of contraction λ. The lower density for large λ is compensated by a larger force contribution from each bridge such that the magnitude of *stress* is roughly independent of λ. Decreasing the relative adhesiveness $k_{-,f}/k_{-,b}$ has only little effect on the average bridge density but shifts the distribution more to the front.

In Ref. [5] the pole force is introduced as a measure for the overall contractile force exerted on the substratum. It is defined as the stress components $\boldsymbol{\sigma} \equiv (\bar{\sigma}_{xz}, \bar{\sigma}_{yz})$ parallel to the substratum integrated over the front half of the cell[5],

$$\boldsymbol{F}_b \equiv \int_{x>x_0} \boldsymbol{\sigma}(x,y)\mathrm{d}A \ . \tag{7}$$

The orientation and origin of the frame of reference are based on experimental data on the cell outline.

Since our model of cell contraction does not explicitly describe the cell outline, we use a slightly different definition of the pole force. In our definition, the pole force at the front is the sum of all (point) forces exerted in the negative direction

$$\boldsymbol{F}_f \equiv k_s \sum_{u_x<0} \boldsymbol{u} = \sum_{\sigma_x<0} \boldsymbol{\sigma} \ . \tag{8}$$

This definition is equivalent to Eq. 7 when the origin $\boldsymbol{x}_0$ is chosen to be the center of contraction, i.e.

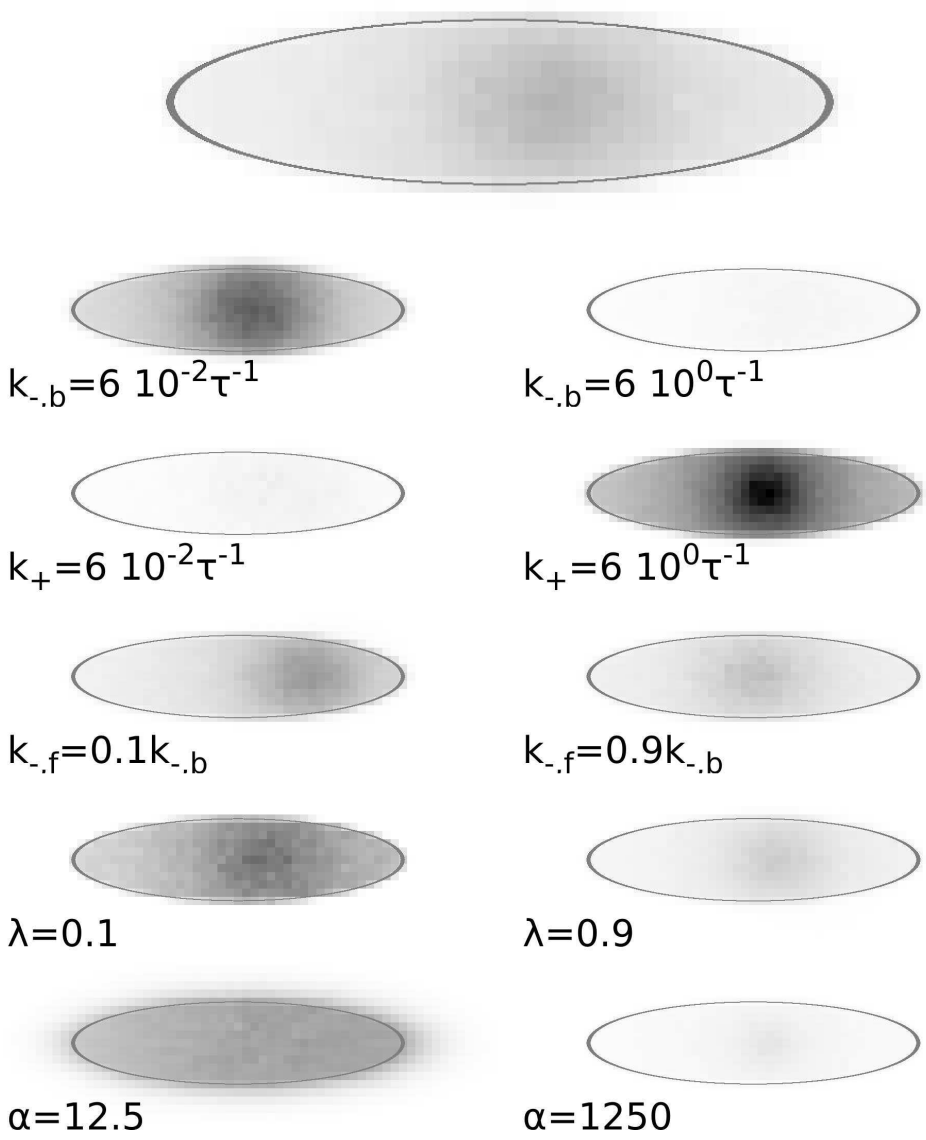

Figure 5: The density of attachments, averaged over an entire contraction cycle, for different sets of model parameters. Black/white corresponds to densities $\approx 2.15\mu\mathrm{m}^{-2}$ and $< 2.15{\cdot}10^{-3}\mu\mathrm{m}^{-2}$, respectively. The time averaging was achieved by rescaling and overlaying the contracted ellipses. The upper pattern corresponds to the default set of parameters: $k_{-,b}$=$6{\cdot}10^{-1}\tau^{-1}$, $k_{-,f}$=$0.5k_{-,b}$, k_{+}=$6{\cdot}10^{-1}\tau^{-1}$, α=125, $\lambda = 0.5$, and $N = 200$. For this set of parameters, the maximal density is $\approx 0.64\mu\mathrm{m}^{-2}$. In each row one model parameter is varied while keeping the remaining parameters fixed.

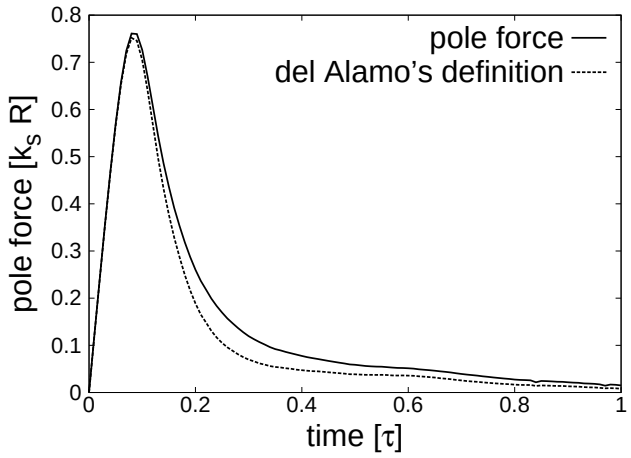

Figure 6: Comparison of pole forces. For the standard parameter set, the definition by del Álamo and our definition yield similar quantitative results.

$u_x(\boldsymbol{x}_0) = 0$. Note, that in the definition Eq. 7 a shift of the reference frame (i.e. the cell outline) leads to lower pole forces as the origin moves away from the center of contraction. In contrast, our definition is independent of the location of the cell outline.

Fig. S6 shows that for the standard parameter set both definitions give qualitatively and quantitatively very similar results. In order to apply Eq. 7 to our simulation data, we chose the center of the contracted ellipse as $\boldsymbol{x}_0$. Note, however, that the center of the contraction area will in general be different from the center of the cell outline.

Fig. S7 shows the average pole force over one contraction cycle as a function of the off-rate. The pole force gives an estimate of the maximal force supported by the binding bridges. As can be seen from Fig. S7, for very large $k_{-,b}$ the detachment force is insufficient to support the traction force that balances the viscous drag of the protruding cell ($\sim$ 0.1pN [5]). For approximately symmetric cells, force balance then implies that a forward protrusion is accompanied by a backward motion of the same order. Hence, there is no net motion for sufficiently large $k_{-,b}$.

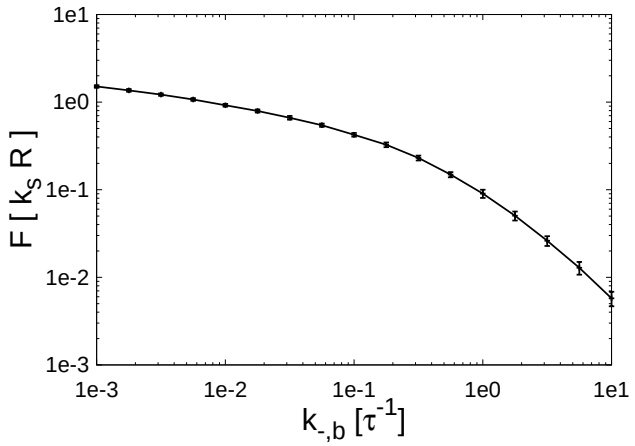

Figure 7: The average pole force exerted during one contraction cycle as a function of $k_{-,b}$.

References

[1] Spudich, J. A., 1994. How molecular motors work. *Nature* 372:515–518.

[2] Debold, E. P., J. B. Patlak, and D. M. Warshaw, 2005. Slip Sliding Away: Load-Dependence of Velocity Generated by Skeletal Muscle Myosin Molecules in the Laser Trap. *Biophys. J.* 89:L34 – L36.

[3] Zhang, W., and D. N. Robinson, 2005. Balance of actively generated contractile and resistive forces controls cytokinesis dynamics. *Proc. Natl. Acad. Sci.* 102:7186–7191.

[4] DiMilla, P. A., K. Barbee, and D. A. Lauffenburger, 1991. Mathematical model for the effects of adhesion and mechanics on cell migration speed. *Biophys. J.* 60:15 – 37.

[5] del Álamo, J. C., R. Meili, B. Alonso-Latorre, J. Rodríguez-Rodríguez, A. Aliseda, R. A. Firtel, and J. C. Lasheras, 2007. Spatio-temporal analysis of eukaryotic cell motility by improved force cytometry. *Proc. Natl. Acad. Sci.* 104:13343–13348.